

Preprint*: Thermal-Hydraulic Analysis of Flow in Rib-Roughened Passages with application to Gas-cooled Nuclear Reactors

A. Keshmiri¹, M.A. Cotton², Y. Addad³ and D. Laurence⁴

School of Mechanical, Aerospace and Civil Engineering, The University of Manchester, Manchester M60 1QD, UK.

¹a.keshmiri@postgrad.manchester.ac.uk

²mark.cotton@manchester.ac.uk

³yacine.addad@manchester.ac.uk

⁴dominique.laurence@manchester.ac.uk

Abstract – The present paper reports RANS simulations of the flow and heat transfer in a 2-dimensional rib-roughened passage. Rib pitch-to-height ratios of 6, 9, and 12 are examined. The blockage ratio of the transversely-mounted rectangular ribs is 10%, making the case ‘very rough’. The Reynolds number, based on the channel bulk velocity and hydraulic diameter, is 30,000. Three low-Reynolds-number linear EVMs, namely the Lien-Chen-Leschziner $k-\varepsilon$ model, the Menter $k-\omega$ -SST model, and a variant of Durbin’s v^2-f formulation are examined. Results for a square rib profile are compared to those for the rib profile used in the fuel pins of Advanced Gas-cooled Reactors. All computations are undertaken using the commercial CFD code ‘STAR-CD’. In comparison with experimental data, it emerges that the v^2-f model generally returns more accurate results than the $k-\varepsilon$ or $k-\omega$ -SST closures.

1. Introduction

Rough surfaces are widely used to enhance convective heat transfer by the promotion of higher turbulence levels. The penalty associated with such roughening is an increase in drag and consequently much effort has been devoted to the optimization of roughness designs.

The principal application of the present work is to the rib-roughened fuel pins of the UK fleet of Advanced Gas-cooled Reactors (AGRs). Results presented below are for a 2D-plane passage, this study forming a precursor to the simulation of the more complex reactor geometry.

Laboratory studies of flow over repeated-rib surfaces date back at least as far as 1950s; see, for example, the discussion of Webb, Eckert and Goldstein [1]. In their own experimental programme Webb et al. investigated pipe flow with repeated rectangular ribs, focusing upon the effects of geometrical factors on flow resistance and heat transfer (Reynolds and Prandtl number effects were also studied). In line with established findings for sand-roughened surfaces (see Schlichting [2] for example), it was found that flow resistance and heat transfer levels increased with relative roughness (i.e. the ratio of rib height to pipe diameter, k/D). Pitch-to-height ratios of $10 \leq P/k \leq 40$ were examined and it was established that flow resistance and heat transfer decreased monotonically as P/k was increased over this range.

The maximum value of relative roughness studied by Webb et al. was $k/D = 0.04$. Han, Glicksman and Rohsenow [3] later conducted experiments on a rectangular channel with rib-roughened upper and lower walls. k/D_e was extended up to 0.102 (the equivalent diameter is defined as $D_e = 4 \times [\text{flow area}] / [\text{wetted perimeter}]$). The work of Han et al. encompassed an examination of the effect of rib cross-section on the flow thermal-hydraulics: it was established that rib profile had a significant effect on the flow resistance, but only a very limited effect on heat transfer. The years from the late-1970s to the present day have witnessed a continuing high level of experimental activity related to flow over ribbed (and other roughened) surfaces. A recent review is given by Jiménez [4] who pays particular attention to very rough surfaces (discussed further below).

*The electronic version of this paper can be found on www.CFDtm.org.

In the CFD simulations reported in Section 3 below, we focus on the data of Rau et al. [5] who employed two geometrically (and dynamically) similar square cross-section test sections: a smaller one for heat transfer measurements and a larger version designed to give good resolution of the flow field. Air was the working fluid, and the Reynolds number based on the bulk velocity and equivalent diameter was fixed at $Re = 30,000$. In both cross-sections square ribs could be mounted on the lower surface only ('1s'; Figure 1), or on both the lower and upper surfaces ('2s'). In all cases, a large blockage ratio was imposed ($k/H = 0.1$) and the surfaces may be considered to have a high degree of roughness. Rau et al. reported 1s channel results for $P/k = 6, 9$, and 12 , while P/k was set to 9 in the 2s section. For comparison, the helical ribs of AGR fuel pins have a pitch-to-height ratio $P/k \approx 5.5 - 6.5$, the exact value depending upon whether pitch is measured normal to the ribs or in the axial direction (Fairbairn [6]).

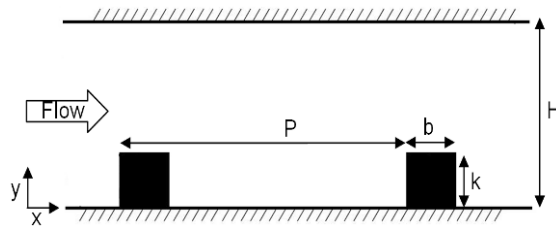


Figure 1 – Schematic diagram of a rib-roughened surface.

Complementing experimental research in the area, the CFD/RANS community has been active in the computation of flow over ribbed surfaces. Acharya et al. [7] used linear and non-linear (quadratic) $k-\varepsilon$ EVMs to make comparison with their own experimental data for flow in a channel with a rib-roughened, and heated, lower wall. The high-Reynolds-number turbulence models were coupled with 'wall functions'. The two models returned similar results; in particular both yielded values of Nusselt number that were significantly lower than the data. This failing is due, at least in part, to the adoption of the wall function approach, it having been established for some time that the strategy performs poorly in separated flows (Rodi [8]).

Low-Reynolds-number forms of the $k-\varepsilon$ model were examined by Iacovides and Raisee [9]. Despite the inclusion of length scale correction terms in the ε -equation, it was found that the models returned too *high* levels of heat transfer for flow over ribbed surfaces, cf. Acharya et al. [7], above. These apparently conflicting findings are discussed further below in the context of the present results.

Ooi et al. [10] employed a form of the v^2-f model that is very similar to the one described in Section 2. A full 3D solution was undertaken in [10]; comparison with the symmetry plane heat transfer data of Rau et al. [5] showed good agreement between the v^2-f model and the measurements. However, model response to secondary flows resulted in poorer results at the channel side-walls.

As noted above, the flow channels studied experimentally by Rau et al. [5], and simulated here, are very rough, with $k/H = 0.1$. Jiménez [4] uses an approximate analysis to show that roughness effects might be expected to extend well into the logarithmic region for flows in which $\delta/k \leq 40$ (or $k/\delta \geq 0.025$; δ is a boundary layer thickness or channel half-width). The extent to which a log layer survives in the present case is examined in Section 3, below.

In relation to AGR fuel channels, the present authors estimate on the basis of design data provided by Fairbairn [6] that k/D_e is an order of magnitude less than the k/H value in the experiments of [5]. Nevertheless, the ratio of k to D_e in AGRs is still sufficiently high to raise the possibility that there will be significant restructuring of the logarithmic layer. (Also, the distance between adjacent fuel pins is somewhat less than D_e ; consequently normalization of k by inter-pin distance will indicate a greater degree of relative roughness.)

2. Physical and Numerical Formulations

2.1 Mean Flow Equations

The mean flow equations for steady and incompressible forced convection flow are written as follows:

Continuity

$$\frac{\partial U_j}{\partial x_j} = 0 \quad (1)$$

Momentum

$$\frac{DU_i}{Dt} = -\frac{1}{\rho} \frac{\partial p}{\partial x_i} + \frac{\partial}{\partial x_j} \left[(v + v_t) \frac{\partial U_i}{\partial x_j} \right] \quad (2)$$

Energy

$$\frac{DT}{Dt} = \frac{\partial}{\partial x_j} \left[\left(\frac{v}{Pr} + \frac{v_t}{\sigma_t} \right) \frac{\partial T}{\partial x_j} \right] \quad (3)$$

The turbulent Prandtl number is set to a constant value, $\sigma_t = 0.9$.

2.2 Numerical Procedures

The commercial code ‘STAR-CD’ [11] is used to generate results using the low-Reynolds-number $k-\varepsilon$ model of Lien, Chen and Leschziner [12] (‘LRN $k-\varepsilon$ model’, below), the $k-\omega$ - SST model of Menter [13] (‘LRN $k-\omega$ - SST model’), and a variant of Durbin’s v^2 - f model due to Iaccarino [14] (‘ v^2 - f model’). In earlier works by the authors and their colleagues, the turbulence models in STAR-CD have been validated against in-house and industrial codes with the same turbulence models [15, 16].

All fluid properties are assumed to be constant. The momentum and turbulence transport equations are discretized using second-order central differencing and first-order upwind differencing schemes, respectively. The energy equation is discretized using the ‘Monotone Advection and Reconstruction Scheme’ (MARS) [11]. The SIMPLE algorithm is adopted for pressure-velocity correction.

A number of carefully-conducted sensitivity tests have been applied to ensure the numerical reliability of the computations.

2.3 Geometry and Grid

The configurations considered here consist of 2-dimensional channels, the lower walls of which are roughened by square ribs of height k . The computational domain is of length $2P$, i.e. it includes 2 ribs. Streamwise periodicity is assumed and cyclic boundary conditions are applied at the inlet and outlet planes. In the 1s case the domain is of height H (Figure 2 (a)), whereas for the 2s channel symmetry permits the use of a domain of height $H/2$ (Figure 2 (b)). The thermal boundary condition at both the lower and upper walls of the 1s case is one of the same uniform wall heat flux. As noted above, the upper boundary of the 2s domain is a symmetry plane.

The rib height to channel hydraulic diameter ratio in the present simulations is $k/D_e = 0.05$, and the blockage ratio (k/H) is 10%. The Reynolds number based on hydraulic diameter is fixed at $Re = 30,000$. Prandtl number is set to 0.71.

There is an unavoidable discrepancy between the square cross-sectioned experimental channel and the present two-dimensional simulations, namely that the equivalent diameter of the square channel is equal to H , whereas $D_e = 2H$ in the 2D case. In order to overcome this difficulty, at least partially, the bulk velocity is set to one-half of the experimental value (and hence the Reynolds numbers based on equivalent diameter are equal). The rib height, k is maintained at the experimental value and therefore the blockage ratio, k/H , rather than k/D_e , is

matched. There remains, however, a lack of geometric similarity, this being due to the differing ratios of ribbed-to-smooth surfaces in the experimental and computational cases (1:3 vs. 1:1 in the 1s case; 1:1 vs. 1:0 for the 2s channel). Finally, as a general observation, it is noted that Rau et al. report significant 3D features in the flow.

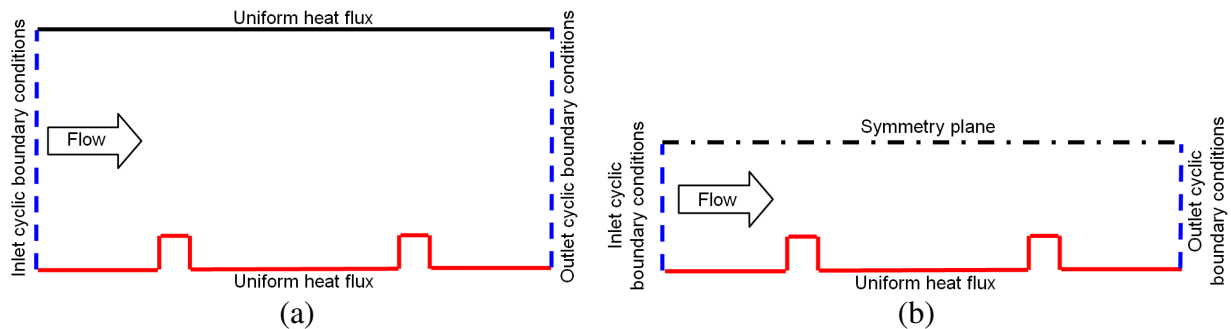


Figure 2 – The computational domains used in the present work: (a) 1s configuration, (b) 2s configuration.

The results presented below were generated using structured Cartesian grids with cell counts of 133,000 ($P/k = 6$), 161,000 ($P/k = 9$), 189,000 ($P/k = 12$), and 111,000 ($P/k = 9$; 2s). Since low-Reynolds-number turbulence models are employed, the grids were generated so as to be very fine near the wall (the wall-adjacent cell typically extends only to $y^+ \leq 0.5$).

The effects of changing the rib profile have also been studied by comparing the ‘Square Rib Profile’ (SRP) above to the rib profile used in the fuel pins of current AGRs. This latter design is known as a ‘Multi-Start Rib Profile’ (MSRP). The mesh used for this case is a structured Cartesian grid with 112,000 cells.

2.4 Turbulence Models

Three turbulence models of the Eddy Viscosity class are examined in the present study. While all three closures eventually trace their roots to the ‘standard’, or ‘parent’, EVM of Launder and Spalding [17], they embody quite distinct modifications to that scheme. The models do, however, share common features in that they are all linear and of the ‘low-Reynolds-number’ type (in common with the widely-adopted extension of the Launder-Spalding scheme proposed by Launder and Sharma [18]). It follows that the systems of governing equations are integrated over the entire flow domain, there being no need to employ wall functions in wall-adjacent regions.

The models as coded into STAR-CD conform to the original published versions (di Mare [19]).

‘Baseline’ k - ε model

The low-Reynolds-number linear version of the k - ε model of Lien, Chen and Leschziner [12] is adopted as a ‘baseline’ formulation against which two more complex EVMs are compared. It is noted that Lien et al. evaluated the effects of including quadratic and cubic elements in the stress/strain relation. Pertinent to the current investigation, the latter form was shown to yield an improved performance in the computation of a separated hill flow. (As part of the wider remit of this work, the present authors intend to examine non-linear EVMs in a subsequent stage of the study.)

The closure of [12] carries two turbulence transport equations, i.e. the k - and ε -transport equations, the latter being somewhat modified from the standard form of [17, 18].

As with the other schemes, the full equations of the Lien et al. model will not be quoted here, and the interested reader is referred to the original work and the STAR-CD manual. It is, however, of importance to highlight the eddy viscosity expression of the model; ν_t is prescribed as

$$v_t = C_\mu f_\mu k^2 / \varepsilon \quad (4)$$

where the ‘damping function’, f_μ reads

$$f_\mu = (1 - \exp(-0.0198 Re_y)) (1 + (5.29/Re_y)) \quad (5)$$

and

$$Re_y = \frac{y\sqrt{k}}{\nu} \quad (6)$$

where y is the normal distance to the closest wall. The use of y in a turbulence model implicitly assumes that the flow possesses features of ‘universality’. It is of particular significance that y is adopted in Eqns. (4)-(6) because the constitutive equation provides the only input from the turbulence field to the mean flow.

k- ω -SST model

The k - ω -SST model is the second two-equation EVM to be considered in the present work. ω , the large-scale turbulence frequency, is broadly equivalent to ε/k . In its essential features the ω -transport equation may be obtained by formally manipulating the k - and ε -equations, although in so doing a cross-diffusion term arises in the ω -equation. That term is omitted in the standard k - ω model (Wilcox [20]), and therefore there is not a strict equivalence between the k - ε and k - ω formulations.

Menter [13] developed a combined k - ω / k - ε model in which a blending function, F_1 is included in the ω -equation. A term $(1-F_1)$ multiplies the ‘exact’ cross-diffusion term discussed above. Thus, when $F_1 \approx 1$ (in the viscous sublayer and logarithmic region of a smooth wall boundary layer) the original ω -transport equation of [20] is recovered. On the other hand, as $F_1 \rightarrow 0$ in the outer flow the model reverts to standard k - ε format. Linear blending as a function of F_1 is also applied to the model constants (these differing in the k - ω and k - ε schemes).

In the same paper Menter proceeded to develop a k - ω -SST (or Shear Stress Transport) model; it is this second formulation that is adopted in the present work. The SST scheme departs from the initial k - ω / k - ε formulation of [13] in terms of the values assigned to the model constants and by virtue of the introduction of a new expression for v_t which includes a dependence on a second blending function, F_2 . It is noted that both F_1 and F_2 are dependent on wall distance, y (cf. the Lien et al. model [12], above)

v^2 - f model

The final model to be considered here is the ‘ v^2 - f model’ which was first proposed by Durbin [21] (v is the wall-normal fluctuating velocity). Damping in the v^2 - f scheme is related to the diminution of the $\overline{v^2}/k$ that occurs as a wall is approached (see Launder [22], for example):

$$v_t = C_\mu \frac{\overline{v^2}}{k} k T \quad (7)$$

The large-scale turbulence timescale is truncated on the Kolmogorov scale,

$$T = \max \left[\frac{k}{\varepsilon}, C_{kT} \left(\frac{v}{\varepsilon} \right)^{0.5} \right] \quad (8)$$

In terms of the number of differential equations carried, the v^2 - f model is the most complex of the schemes to be examined here. Equations for k - and ε -transport are complemented by an

equation for $\overline{v^2}$ -transport and an elliptic relaxation equation for f_{22} , a re-distribution term that appears in the $\overline{v^2}$ -equation.

The form of the v^2 - f model implemented in STAR-CD is that given by Iaccarino [14]. The v^2 - f formulation is the only one of those to be examined here *not* to include any direct dependence on wall distance. (In fact, in an earlier version of the general form of [14], Durbin [23] included a y -dependent function in the production term of the ε -equation, but that was subsequently modified by Iaccarino to eliminate wall distance dependence.)

3. Results and Discussion

3.1 Performance of the Turbulence Models

Local Nusselt number is defined here as

$$Nu = \frac{\dot{q} D_e}{\lambda (T_w - T_b)} \quad (9)$$

As in Rau et al. [5], all Nusselt number distributions for the ribbed duct calculations are normalized by the value associated with a smooth passage (the Dittus-Boelter equation):

$$Nu_0 = 0.023 Re^{0.8} Pr^{0.4} \quad (10)$$

Figure 3 compares the heat transfer results of the k - ε , k - ω - SST , and v^2 - f models with the experimental data of [5] for the 1s channel with $P/k = 12$. The region of maximum heat transfer corresponds to the location of the re-attachment point (compare Figures 3 and 4). The k - ε model clearly returns levels of heat transfer that are far too high. Such a result might be anticipated from the findings of Iacovides and Raisee [9]: the length scale correction they employed in combination with a low-Reynolds-number k - ε model acts to increase ε and thus reduce ν_t (however Nu was still over-predicted, albeit by a smaller margin than that seen here).

The turbulence length scale plays a critical role in the computation of separated flows. It was remarked in the Introduction that the use of a high-Reynolds-number k - ε model coupled with wall functions (Acharya et al. [7]) gave rise to an *under*-prediction of heat transfer levels. The same result was found when a k - ε model was blended with a near-wall k - l form (l being a prescribed length scale; Iacovides [24] and Ooi et al. [10]). In fact, there are two related mechanisms at work – one alluded to already that concerns the diffusivity of the thermal field, and the other is an ‘indirect’ effect related to the mean dynamic field and hence the advective terms of the Energy Equation, Eqn. (3). This point is expanded below in connection with Figure 6.

The k - ω - SST model is closer than the k - ε model to the data in Figure 3, but it is the v^2 - f formulation that is in the closest, although still not excellent, accord with the measurements. Ooi et al. [10] made comparison with the data of [5] using a v^2 - f formulation that differs only slightly from the present form (Section 1, above). The 3D computations of [10] for $P/k = 12$ returned a Nusselt number distribution on the line of symmetry of the channel floor that was around 15% *lower* than the data, cf. Figure 3. (However, the results of [10] for $P/k = 9$ showed only a slight under-prediction of the data.) The discrepancy between the findings of Ooi et al. and Figure 3 gives some measure of the errors incurred by the present adoption of a 2D computational framework.

Figure 5 shows the normalized streamwise velocity for $P/k = 9$ at one-tenth of the rib height. The recirculation region and re-attachment point are evident in the data and the v^2 - f and k - ε model results, while the k - ω - SST model indicates that the flow remains reversed at this elevation. The k - ω - SST model therefore fails to predict flow renewal in the inter-rib cavity and consequently its relatively good agreement with the heat transfer data of Figure 3 must be viewed as being largely fortuitous.

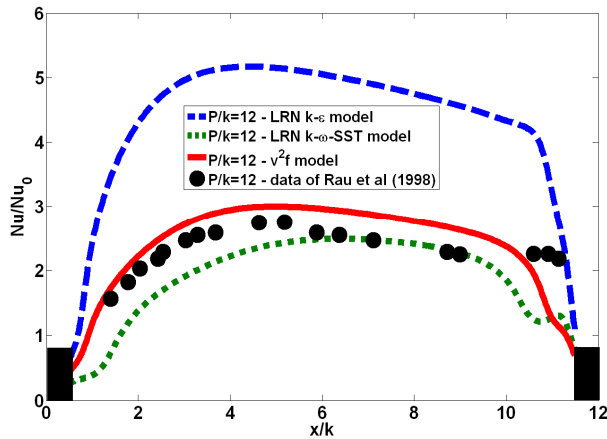


Figure 3 – Nusselt number distributions for $P/k = 12$.

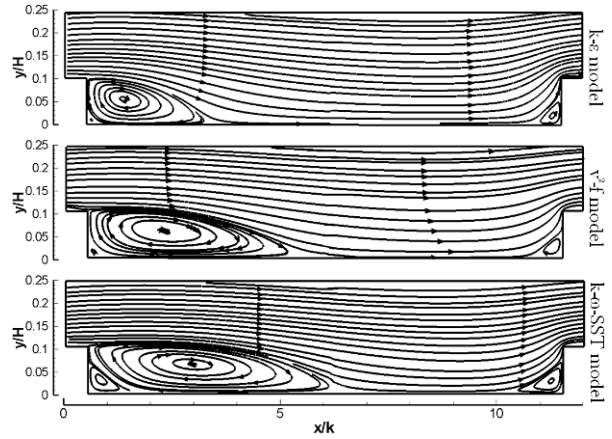


Figure 4 – Streamlines for $P/k = 12$.

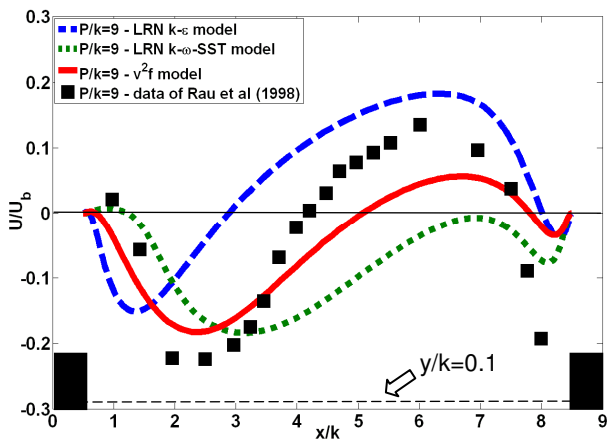


Figure 5 – Streamwise velocity distributions for $P/k = 9$; 1s at $y/k = 0.1$.

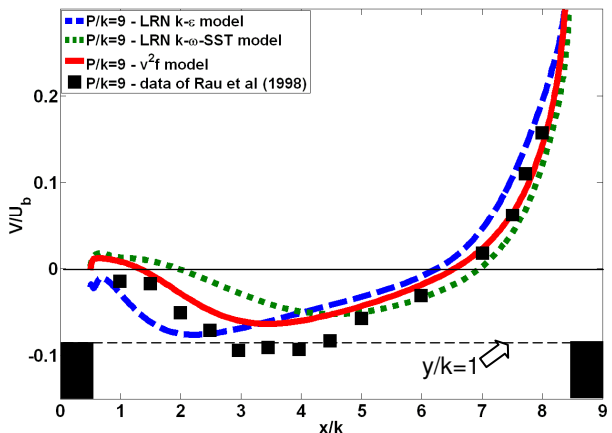


Figure 6 – Wall-normal velocity distributions for $P/k = 9$; 1s at $y/k = 1$.

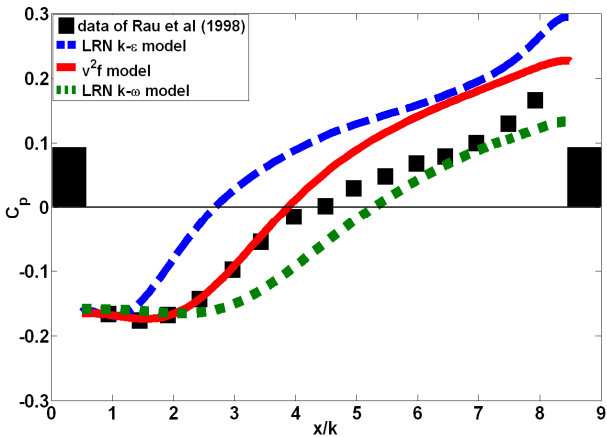


Figure 7 – Pressure coefficient distribution for $P/k = 9$; 1s.

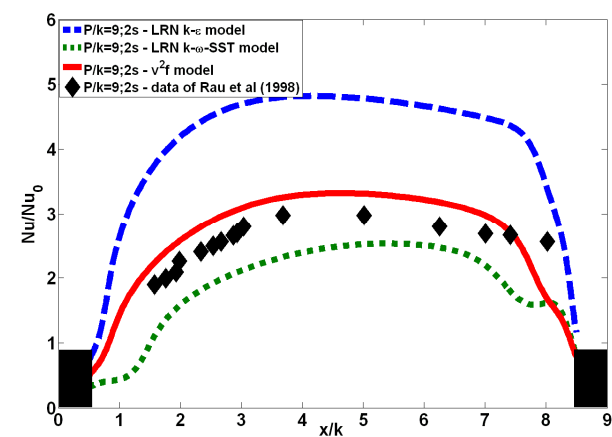


Figure 8 – Nusselt number distributions for $P/k = 9$; 2s.

Results for the wall-normal velocity at rib height are presented in Figure 6. The v^2-f model is in reasonably good agreement with the data as, to a somewhat lesser degree, is the baseline $k-\epsilon$ formulation. The $k-\omega-SST$ model generally under-predicts the magnitude of the wall-directed velocity. Comparing Figures 6 and 3, it is seen that there is a direct correspondence between the magnitude of the downward-going velocity in the recirculation region and the level of heat transfer. This raises the question of the importance of advection in determining the thermal characteristics of recirculating flows, i.e. in a mathematical sense there is now a focus on the left hand side of Eqn. (3). First, it is remarked that identical mean flow equations

are employed in conjunction with the three turbulence models considered here, and that the only input of a turbulence model to Eqns. (2) and (3) is the turbulent viscosity, ν_t . The discussion above has identified the importance of the turbulence length scale as a determinant of model performance. It is clear though that the length scale exerts an influence on the thermal field via its role in the *dynamic* field (the right hand side of Eqn. (2)). Thus, in relation to the Energy Equation, length scale effects are manifest indirectly via the advective terms and directly via turbulence diffusion.

Attention is turned next to the inter-rib pressure distribution. Impingement on the upstream face of the rib leads to high static pressure, while there is a low pressure zone downstream of the rib. These effects can be seen in Figure 7, where the pressure coefficient distribution between the two ribs is plotted against x/k for $P/k = 9$. The pressure coefficient is defined as

$$C_p = \frac{P - P_{ref}}{0.5\rho U_b^2} \quad (11)$$

where p is the static pressure on the wall and p_{ref} is a reference pressure. (Note that C_p for all three models is offset to the experimental value at $x/k = 0.5$.) Figure 7 shows that the $k-\varepsilon$ model overestimates C_p , whereas the $k-\omega$ -SST model returns values that are too low. Within the recirculation zone, at least, the v^2 - f model is in good agreement with the data.

Heat transfer results for the $k-\varepsilon$, $k-\omega$ -SST, and v^2 - f models for the 2s channel with $P/k = 9$ are shown in Figure 8. The findings are similar to those of Figure 3, and it can be seen that, while the v^2 - f model is in quite close agreement with the data, the $k-\varepsilon$ and $k-\omega$ -SST models over-predict and under-predict the results, respectively.

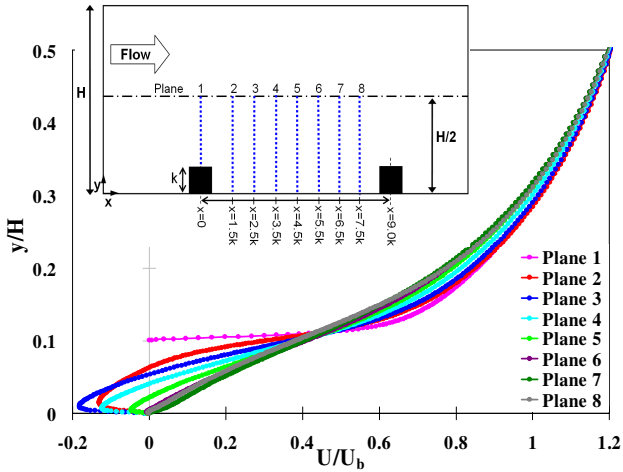


Figure 9 – Velocity profiles plotted on linear axes ($P/k = 9$; v^2 - f model).

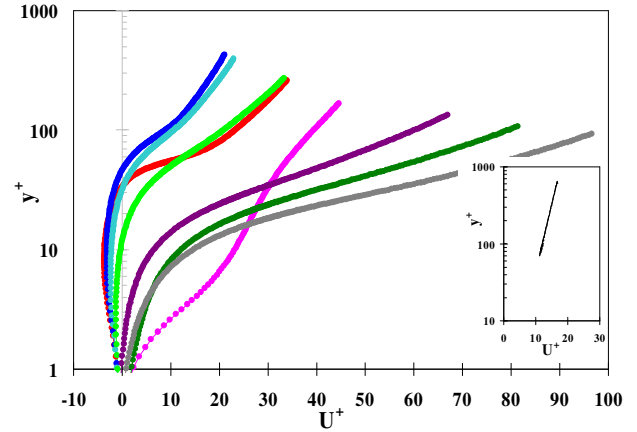


Figure 10 – Velocity profiles plotted on semi-logarithmic axes ($P/k = 9$; v^2 - f model).

Figure 9 shows velocity profiles at a number of monitoring planes on, and between, two ribs. Here $P/k = 9$ and the v^2 - f model is employed. The recirculation region (Planes 2-5) may be identified and the profiles in the recovery region (Planes 6-8) are characteristic of a laminar, rather than a turbulent boundary layer.

An alternative presentation of the velocity profiles is given in Figure 10 which shows $U^+ = U/U_\tau$ vs. $y^+ = yU_\tau/\nu$ plotted on semi-logarithmic axes. (The local friction velocity is defined as $U_\tau = \sqrt{|\tau_w|/\rho}$.) As would be expected, the flow is highly ‘non-universal’ within the separation bubble (for comparison, the inset to Figure 10 shows the conventional ‘law of the wall’). It is now seen more clearly that the recovery region takes the form of a developing laminar boundary layer (here large U^+ is associated primarily with low values of U_τ).

3.2 Effects of varying the Rib Pitch-to-Height Ratio

The remaining results to be presented are for 1s channels and all computations are undertaken using the v^2-f model.

Figure 11 compares heat transfer levels for various P/k ratios. In general, it is seen that the v^2-f model tends to overestimate levels of heat transfer. The model returns the least accurate results for $P/k = 6$, where it over-predicts heat transfer levels by approximately 50%. The most accurate results are for $P/k = 9$.

Streamlines for all three P/k ratios are shown in Figure 12. This figure indicates that there is no re-attachment point for $P/k = 6$, a result that is in agreement with the data (Figure 13 below). The recirculation lengths for $P/k = 9$ and 12, are nearly the same; however, the model over-predicts the measurements of Rau et al. [5].

Figure 13 shows normalized streamwise velocity distributions at $y/k = 0.1$. The v^2-f model underestimates the velocity magnitude in the separation region before the downstream rib. Consistent with Figure 12, there is no re-attachment of the flow for $P/k = 6$.

Results for the wall-normal velocity at rib-height are presented in Figure 14. Except for $P/k = 12$, the v^2-f model is in close agreement with the data.

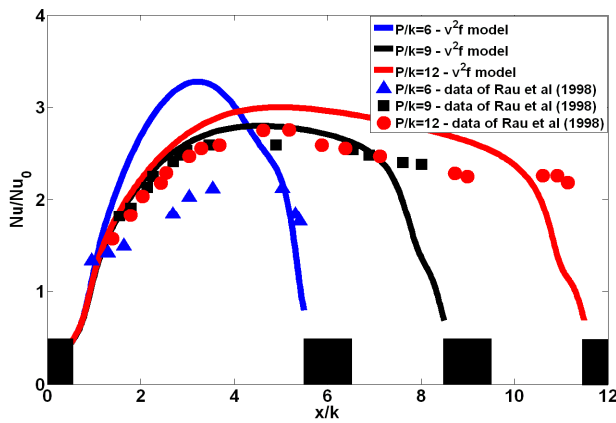


Figure 11 - Nusselt number distributions for $P/k = 6, 9$ and 12 using the v^2-f model.

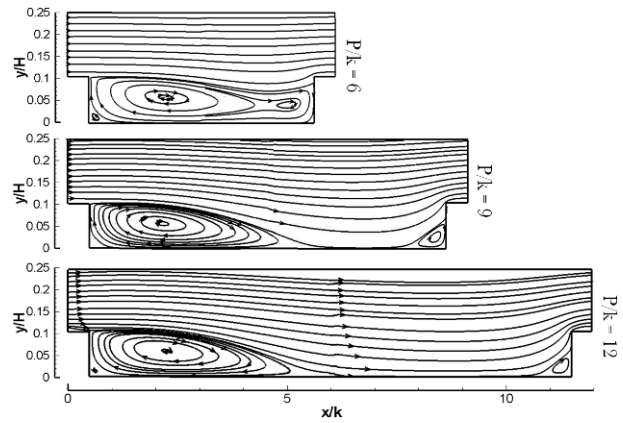


Figure 12 - Streamlines for $P/k = 6, 9$ and 12 using the v^2-f model.

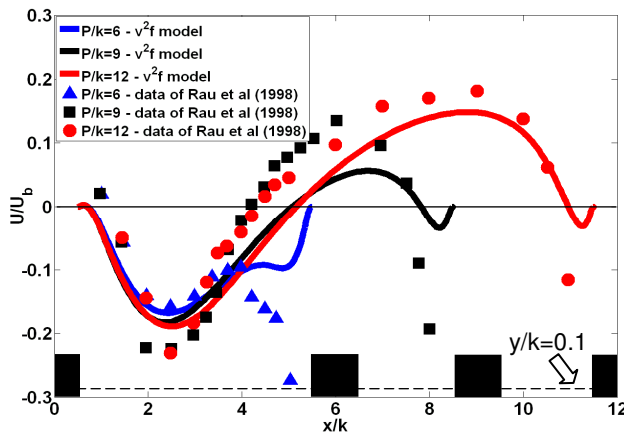


Figure 13 – Streamwise velocity distributions for $P/k = 6, 9$ and 12 at $y/k = 0.1$.

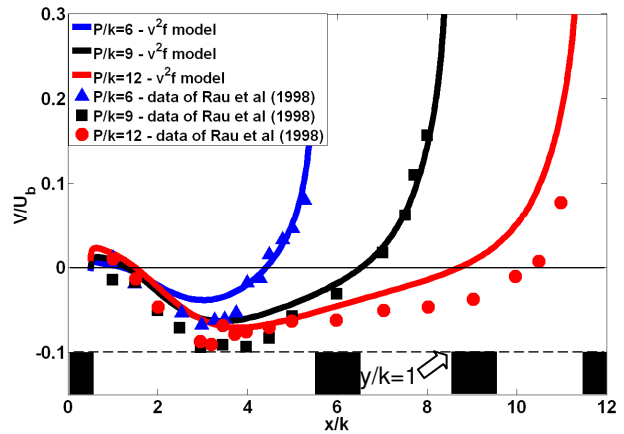


Figure 14 – Wall-normal velocity distributions for $P/k = 6, 9$ and 12 at $y/k = 1$.

3.3 Effects of alternative Rib Profiles

Figure 15 examines the effect of rib profile on heat transfer performance. A Square Rib Profile (SRP, as in Figure 3) and AGR-type Multi-Start Rib Profile (MSRP) are considered. There is little effect on the Nusselt number distribution, and indeed it was noted in Section 1 above that Han et al. [3] found that changes to the rib cross-section had only a strictly limited effect on heat transfer levels.

Figure 16 shows broadly similar streamlines for both rib profiles, although the recirculation length for the SRP is slightly larger than that for the MSRP.

Figures 17 and 18 compare normalized streamwise and wall-normal velocity distributions, and again it is seen that the v^2 - f model returns similar results for the SRP and MSRP cases.

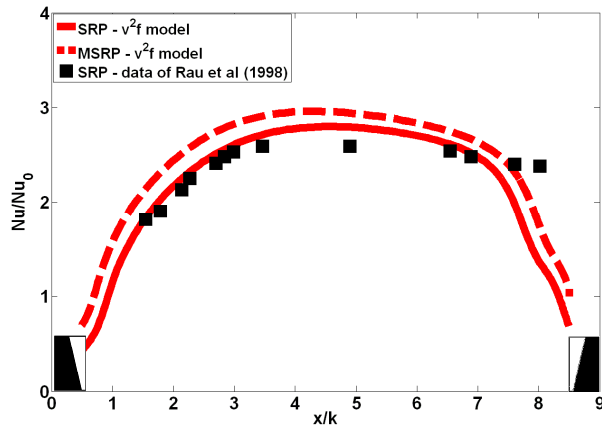


Figure 15 – Nusselt number distributions for $P/k = 9$ and different rib profiles using the v^2 - f model.

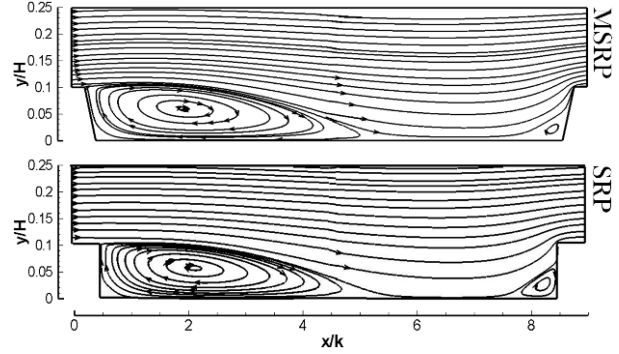


Figure 16 – Streamlines for $P/k = 9$ and different rib profiles using the v^2 - f model.

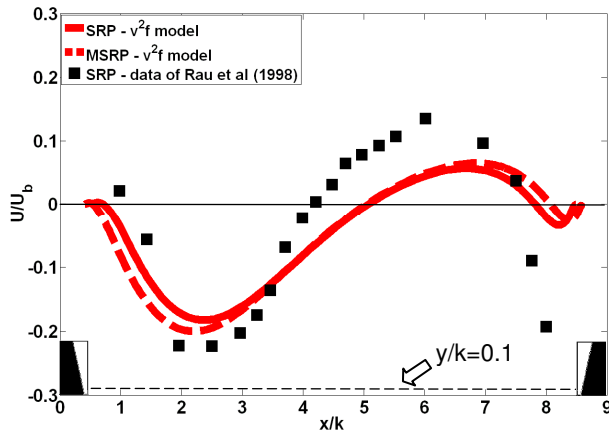


Figure 17 – Streamwise velocity distributions for $P/k = 9$ at $y/k = 0.1$ for different rib profiles.

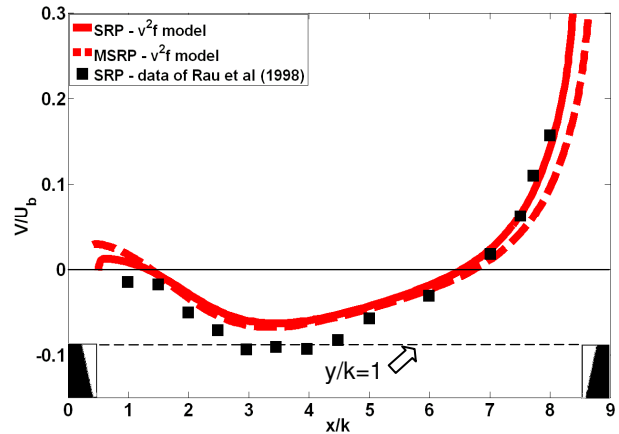


Figure 18 – Wall-normal velocity distributions for $P/k = 9$ at $y/k = 1$ for different rib profiles.

4. Concluding Remarks

Numerical simulations of the flow and heat transfer in 2-dimensional rib-roughened ducts have been performed using the Lien-Chen-Leschziner k - ϵ model, the Menter k - ω - SST model, and a variant of Durbin's v^2 - f formulation. All simulations were undertaken using a commercial CFD package, 'STAR-CD'. Configurations with rib pitch-to-height ratios of 6, 9, and 12 were studied. Of the three models, the v^2 - f model was found to be in the best agreement with the dynamic and thermal field data of Rau et al. [5].

The preceding remarks must be qualified by noting that the present study adopts a 2D framework, whereas the importance of 3D effects is noted in [5]. Furthermore, there is an unavoidable disparity in terms of geometric similarity (this being related to the ratios of ribbed-to-smooth wall areas in the experiments and computations). It is also recorded that there has been no evaluation of Reynolds number effects, although it is known that turbulence models applied to recirculating flows display Reynolds number sensitivity (Iacovides and Raisee [9]).

The wide variation in turbulence model performance is attributed primarily to model determination of the turbulence length scale, and the role of the length scale in affecting both

the advective and diffusive terms of the Energy Equation is discussed in the main text. It is pertinent to consider the reliance a turbulence model places on wall distance, y to represent the turbulence scale (since the use of y carries with it implicit assumptions of universality). It is noted that the k - ε model of [12] has a strong dependence on y since the wall distance appears in the constitutive equation and hence feeds directly into the mean field; y also plays a role in the k - ω - SST model [13] by virtue of its use in blending functions employed in the ω -equation and expression for ν_t . The ν^2 - f model [14] is unique amongst those considered here in having no dependence on wall distance.

ν^2 - f computations indicate that there is little difference between the thermal performance of channels with square ribs and those with AGR rib profiles.

It is evident that the ‘very rough’ rib-roughened surface considered here gives rise to highly non-universal flow features. This has implications both for the use of wall functions in turbulence model computations and, more fundamentally, for the representation of the surface as a distributed ‘sand grain’ type of boundary.

In a subsequent stage of the study, the present authors intend to examine other turbulence models including non-linear EVMs, and also plan to use Large Eddy Simulation techniques to simulate the 3D test case of [5]. Finally, the conclusions which have emerged from the present ‘parametric’ study will inform the simulation of flow over accurately represented AGR fuel elements.

Acknowledgements

The authors are grateful to the UK Engineering and Physical Sciences Research Council for providing funding under grant EP/C549465/1, ‘Keeping the Nuclear Option Open’ (KNOO). Mr. J. Gotts and Dr. S.A. Fairbairn of British Energy kindly supplied information concerning AGR design and operating conditions. Dr. F. di Mare of CD-adapco shared her detailed knowledge of the turbulence models implemented in STAR-CD. Finally, we are pleased to acknowledge the value of discussions with our colleagues Professor H. Iacovides and Dr. T.J. Craft.

References

- [1] R.L. Webb, E.R.G. Eckert and R.J. Goldstein. Heat transfer and friction in tubes with repeated-rib roughness. *Int. J. Heat Mass Transfer*, 14: 601-617, 1971.
- [2] H. Schlichting. *Boundary-layer Theory*. 7th ed. McGraw Hill, New York, 1979.
- [3] J.C. Han, L.R. Glicksman and W.M. Rohsenow. An investigation of heat transfer and friction for rib-roughened surfaces. *Int. J. Heat Mass Transfer*, 21: 1143–1156, 1978.
- [4] J. Jiménez. Turbulent flows over rough walls. *Annual Review of Fluid Mechanics*, 36: 173–196, 2004.
- [5] G. Rau, M. Çakan, D. Moeller and T. Arts. The effect of periodic ribs on the local aerodynamic and heat transfer performance of a straight cooling channel. *ASME J. Turbomach.*, 120: 368–375, 1998.
- [6] S.A. Fairbairn. Personal communication, 2009.
- [7] S. Acharya, S. Dutta, T.A. Myrum and R.S. Baker. Periodically developed flow and heat transfer in a ribbed duct. *Int. J. Heat Mass Transfer*, 36: 2069-2082, 1993.
- [8] W. Rodi. Experience with two-layer models combining the k - ε model with a one-equation model near the wall. *AIAA Paper 91-0216*, 1991.
- [9] H. Iacovides and M. Raisee. Computation of flow and heat transfer in two-dimensional rib-roughened passages, using low-Reynolds-number turbulence models. *Int. J. Numerical Methods for Heat and Fluid Flow*, 11: 138-155, 2001.
- [10] A. Ooi, G. Iaccarino, P.A. Durbin and M. Behnia. Reynolds averaged simulation of flow and heat transfer in ribbed ducts. *Int. J. Heat Fluid Flow*, 23: 750–757, 2002.
- [11] CD-adapco. STAR-CD Methodology, Version 4.02, 2006.

- [12] F.S. Lien, W.L. Chen and M.A. Leschziner. Low-Reynolds-number eddy-viscosity modelling based on non-linear stress-strain/vorticity relations. In: *Proc. 3rd Int. Symp. on Engineering Turbulence Modelling and Experiments (Eds. W. Rodi and G. Bergeles)*, Crete, Greece, pp. 91–100, 1996.
- [13] F.R. Menter. Two-equation eddy-viscosity turbulence models for engineering applications. *AIAA J.*, 32: 1598–1605, 1994.
- [14] G. Iaccarino. Predictions of a turbulent separated flow using commercial CFD codes. *J. Fluids Eng.*, 123: 819-828, 2001.
- [15] A. Keshmiri, M.A. Cotton, Y. Addad, S. Rolfo and F. Billard. RANS and LES investigations of vertical flows in the fuel passages of gas-cooled nuclear reactors. In: *Proc. 16th ASME Int. Conf. on Nuclear Engineering, 'ICONE16', Paper ICONE16-48372*, Orlando, Florida, USA, 2008.
- [16] A. Keshmiri, Y. Addad, M.A. Cotton, D.R. Laurence and F. Billard. Refined eddy viscosity schemes and large eddy simulations for ascending mixed convection flows. In: *Proc. 4th Int. Symp. on Advances in Computational Heat Transfer, 'CHT08', Paper CHT-08-407*, Marrakech, Morocco, 2008.
- [17] B.E. Launder and D.B. Spalding. The numerical computation of turbulent flows. *Comp. Meth. in Appl. Mech. and Eng.*, 3: 269–289, 1974.
- [18] B.E. Launder and B.I. Sharma. Application of the energy dissipation model of turbulence to the calculation of flow near a spinning disc. *Lett. Heat Mass Transfer*, 1: 131-138, 1974.
- [19] F. di Mare. Personal communication 2008.
- [20] D.C. Wilcox. Turbulence Modeling for CFD. DCW Industries Inc., La Cañada, California, 1993.
- [21] P.A. Durbin. Near-wall turbulence closure modeling without damping functions. *Theoret. Comput. Fluid Dynamics*, 3: 1-13, 1991.
- [22] B.E. Launder. Low-Reynolds-Number Turbulence Near Walls. Dept. of Mechanical Engineering, UMIST (now School of MACE, The University of Manchester) Report TFD/86/4, 1986.
- [23] P.A. Durbin. Separated flow computations with the $k-\epsilon-v^2$ model. *AIAA J.*, 33: 659-664, 1995.
- [24] H. Iacovides. Computation of flow and heat transfer through rotating ribbed passages. *Int. J. Heat Fluid Flow*, 19: 393-400, 1998.